Electronic Supplementary Material (ESI) for Nanoscale.

Supplementary Information

Continuous flow chemical vapour deposition of carbon nanotube sea urchins

Jean de La Verpilliere[1], Sarah Jessl[1], Khuzaimah Saeed[1], Caterina Ducati[2], Michael De Volder[1], Adam Boies[1]*

[1]University of Cambridge, Department of Engineering, Cambridge CB2 1PZ, United Kingdom

[2]University of Cambridge, Department of Material Science and Metallurgy, Cambridge CB3 0FS, United Kingdom

**Corresponding author.* Tel: +44(0)1223 332600. E-mail: a.boies@eng.cam.ac.uk

SI 1 Methods

Materials and apparatus

Aluminium and iron nitrate (99.9% purity) and type II deionized water were purchased from Sigma-Aldrich. Silica crystals used as desiccant in the silica gel drier were purchased from GeeJay Chemicals Ltd. All gasses are BOC 99.99% purity compressed gases controlled with mass flow controllers. Both furnaces are electrical tube furnaces with ~ 50 cm heated lengths, equipped with 1 m long, 19 mm inner diameter alumina worktubes.

Characterisation

The powder analysed by XRD was loaded on a 10 mm diameter sample holder and analysed using a Bruker D8 theta/theta diffractometer operated with a Cu Kα radiation source with $2\theta = 10\text{-}80°$ at a scan rate of 0.3°/min (2θ) and a step size of 0.019° (2θ).

Particles collected for SEM imaging and EDX spectroscopy were analysed using a LEO Gemini 1530VP SEM. For EDX analysis, the SEM was operated at 18 kV with a 8 mm working distance.

Scanning transmission electron microscopy was performed on Cu-supported holey carbon grids (Agar Scientific) in a Hitachi S5500 STEM operated at 30 kV in bright field mode.

Raman spectroscopy (EZRaman–N, 532 nm, 50mW) was performed with 5 accumulations of 20 s for each sample.

SI 2 Particle effective density measurement using a tandem DMA-CPMA setup

The aerosol neutraliser used in this study was a TSI 3087 soft X-ray neutraliser. The differential mobility analyser was a TSI 3081 DMA, and the condensation particle counter was a TSI 3076 CPC operated in high flow mode.

Neglecting multiple-charge effects, monodisperse particle bearing one positive elementary charged exit the DMA as shown on Fig. 2. Their mass distribution was then measured by the CPMA, scanning through ~10 particle mass settings. Both the rotation speed and voltage were stepped, resulting in a constant resolution ~ 10 across the CPMA range, as defined by Graves et al. [1s]. Assuming that the effective density is constant for a given mobility, which is reasonable considering the narrow transfer function of the DMA, the CPMA measures a mass distribution whose arithmetic mean is the average particle mass for a given mobility equivalent diameter. Multiply-charged particles result in a second mode that can be resolved as well. In order to extract this average mass, a least-squares minimisation fit was performed with a lognormal distribution as reported by Tajima et al. [2s].

SI 3 XRD results

Table S1: Quantification of XRD results. d_S refers to the crystallites Scherrer size and x_H refers to the proportion of hercynite in the solid solution according to Veggard’s rule.

Peak	**2θ [°]**	**I [%]**	**Plane**	**d_S [nm]**	**x_H [%]**
1	30.53	37.13	[220]	6.88	50
2	36.01	100	[311]	5.79	55.3
3	44.11	33	[400]	7.9	78.7
4	64	40.96	[440]	7.24	69.8

SI 4 Growth optimisation to nominal conditions

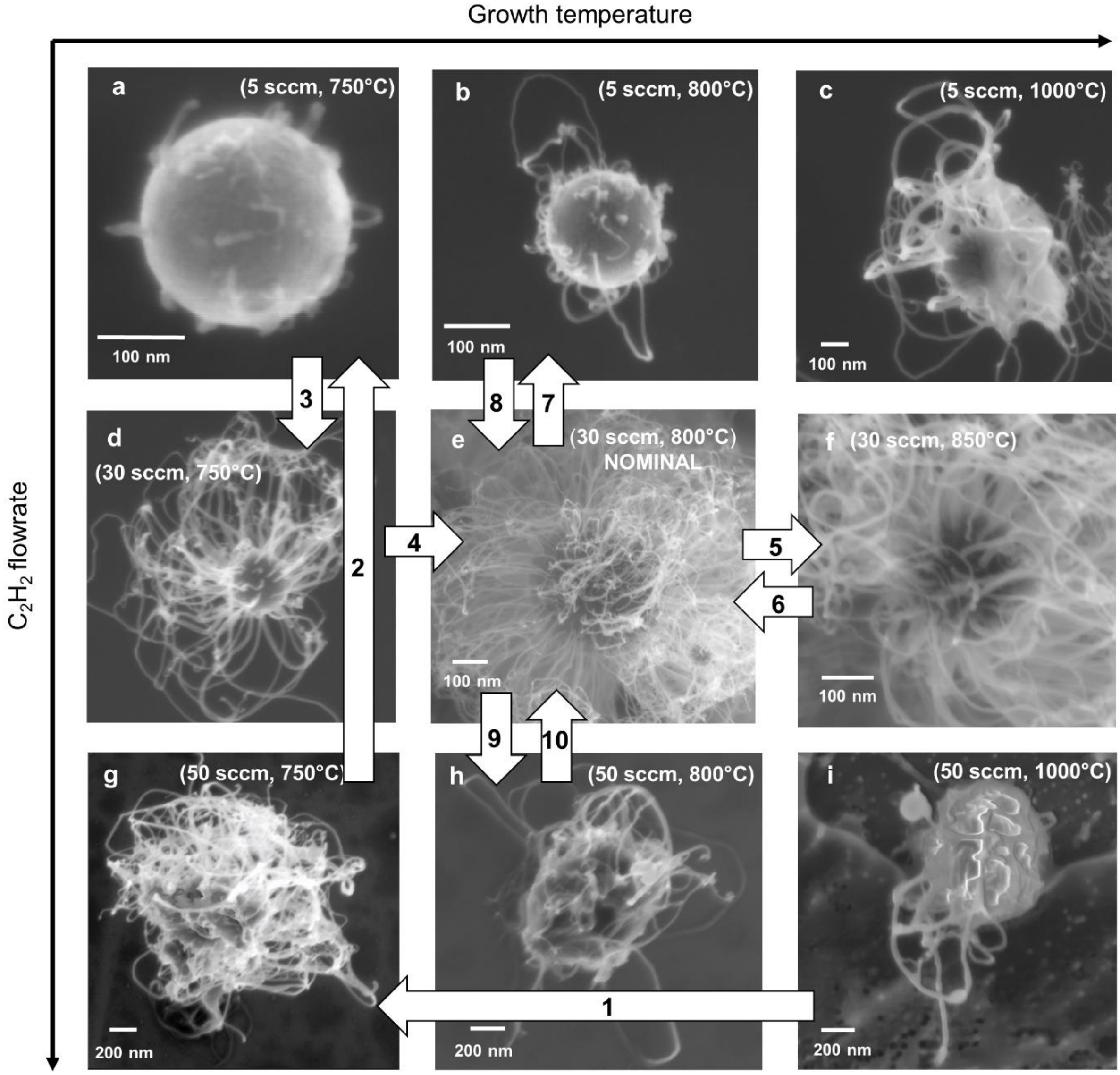

Fig. S1: SEM images of individual CNTSUs at different growth conditions, and example of a typical optimisation iteration strategy to reach nominal conditions illustrated by numbered arrows.

SI 5 Aerosol growth of CNTSUs from smaller diameter cores

As reported previously [3s], we found that CNT growth from small cores (d_p< 40 nm) resulted into CNT structures whose morphologies differ from that of CNTSUs grown on larger cores (see Fig. 5). Fig. S2 shows such a structure grown from a $d_p \approx 40$ nm core at nominal conditions.

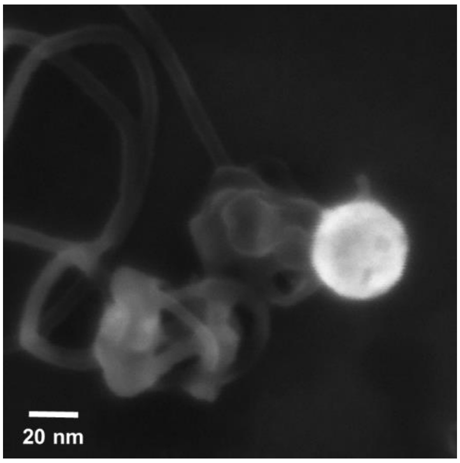

Fig. S2: SEM image of a CNT structure grown from a $d_p \approx 40$ nm core at nominal conditions.

SI 6 Thermogravimetric analysis of aerosol-grown CNTSUs

Thermogravimetric analysis (TGA) was performed on 20 mg of cores collected downstream of furnace 2 at nominal conditions but without acetylene to avoid the formation of CNTs, and on 20 mg of CNTSUs collected downstream of furnace 2 at nominal conditions. The instrument was a Perkin Elmer Pyris TGA with a 20 mL/min flow of synthetic air. Both samples were first held at 100°C for 10 min to remove any moisture, then heated from 100°C to 750°C at 10°C/min, and finally held at 750°C for 10 min. Results are presented in Fig. S2.

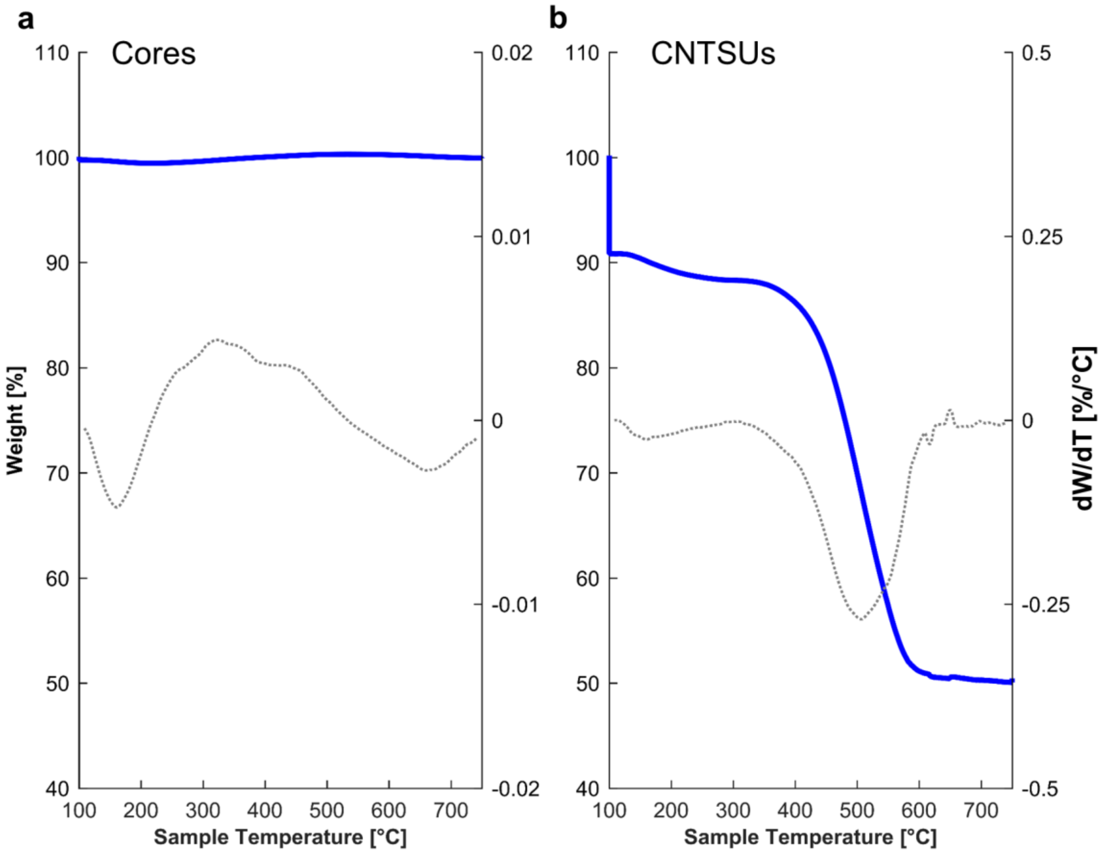

Fig. S3: Thermogravimetric analysis of (a) cores and (b) CNTSUs at nominal conditions. Fraction of initial weight (plain blue, left axis) and relative weight variation rate (dotted grey, right axis).

SI 7 High resolution transmission electron microscopy of aerosol-grown cores and CNTSUs

High resolution transmission electron microscopy (HRTEM) was conducted to analyse the aerosol-grown core materials absent CNT grown (no acetylene addition) and core materials with CNTs grown radially from their core. HRTEM was most informative for smaller (<100 nm) core materials through which the electron beam was able to penetrate. Analysis indicated that the particles are primarily shells with a thickness of ~10% of the overall diameter as shown in Fig. S4. The intensity scan shows in Fig. S4 (top right) that the gray value is not parabolic as would be expected for solid particles, but instead shows particles of varying contrast which is indicative of shell of varying chemistries. Analysis of the lattice spacing of various portions of the core materials indicate the majority of the crystalline material has spacing of ~0.46-0.5 nm, which is representative of metal oxides (AlO_x and $Al_xFe_yO_z$) as shown in Fig. S4 (bottom right). Small portions of the cores have smaller spacings (~0.3 nm) which indicate metallic iron, likely produced during the H_2 reduction in the 2nd furnace.

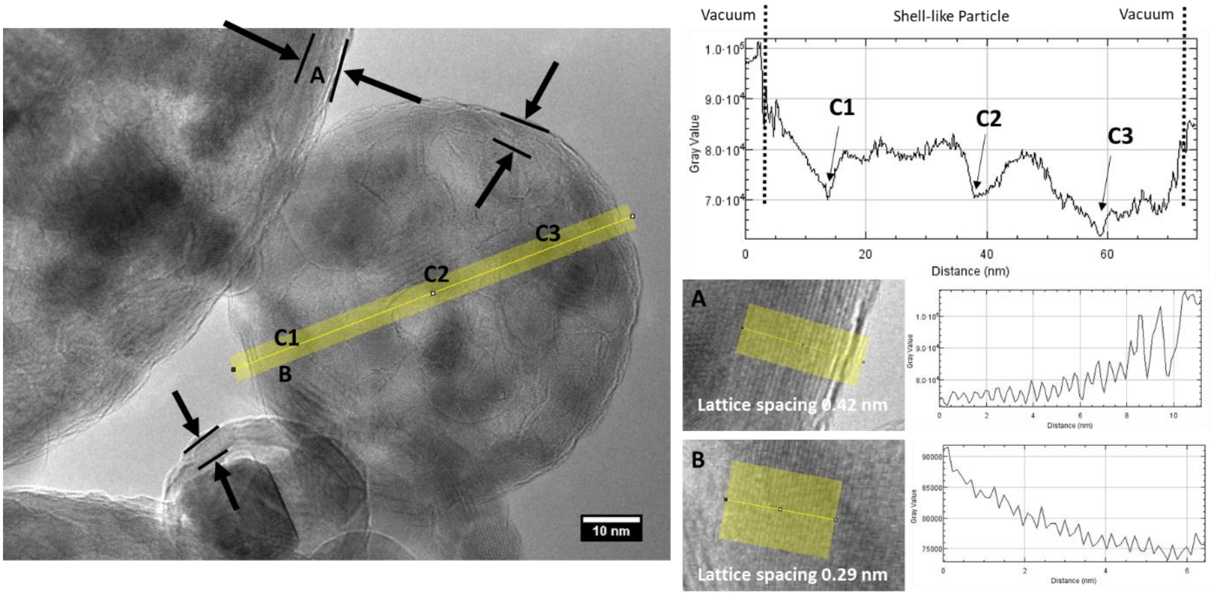

Fig. S4: HRTEM analysis of metal oxide cores absent the growth of CNTs from the surface (no acetylene added) collected after furnace 2. Intensity profiles (right) show the crystallite sizes (C1, C2, C3) and lattice spacing of core materials.

HRTEM of particles from which CNTs had been grown, CNTSUs, demonstrate that the CNTs nucleate (so far as HRTEM allows to probe) from metallic iron, as shown in Fig. S4. The majority of the core particle is metal oxide as demonstrated by multiple analyses of the particle core lattice spacing. The CNTs are anchored to the core material by an iron/iron-carbide catalyst site that serves to produce a MWCNT of ~10 of walls.

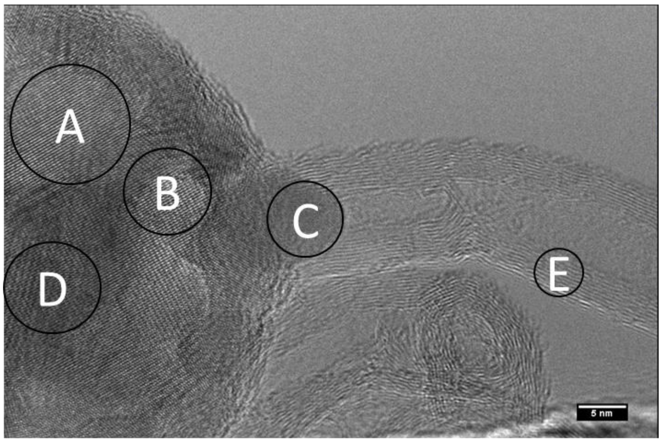

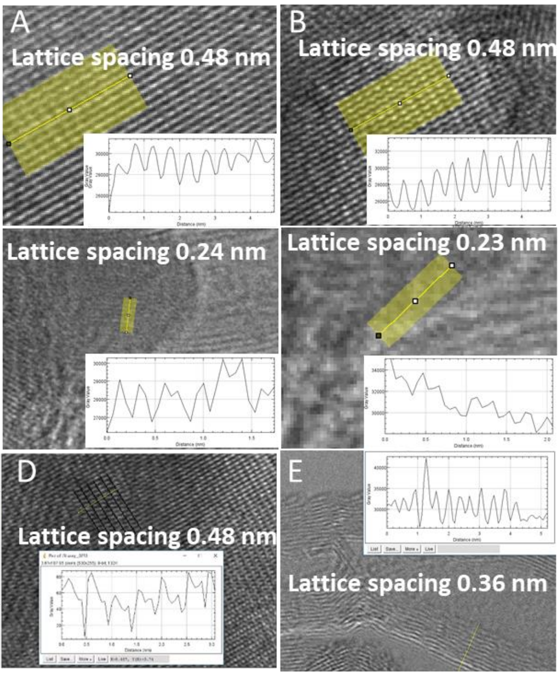

	Magnetite	Maghemite	Hercynite	Hematite	Aluminum Oxide	Wustite	Aluminum	Iron Carbide	CNT-Walls	Iron
	F_3O_4	γ-Fe_2O_3	$FeAl_2O_4$	α-Fe_2O_3	Al_2O_3	$Fe_{x-1}O$	Al	Fe-C	C	Fe
Lattice Parameter [nm]	0.84	0.83	0.82	0.5	0.48	0.43	0.4	0.36	0.34	0.29

Fig. S5: HRTEM analysis of metal oxide core with Fe surface catalyst from which the CNT grows. Intensity profiles (right) show the gray values of crystalline materials throughout the core, which confirms a primarily metal oxide core (~0.48 nm), metallic or iron-carbide CNT catalyst site (~0.23 nm) and MWCNTs with spacing of (~0.36 nm).

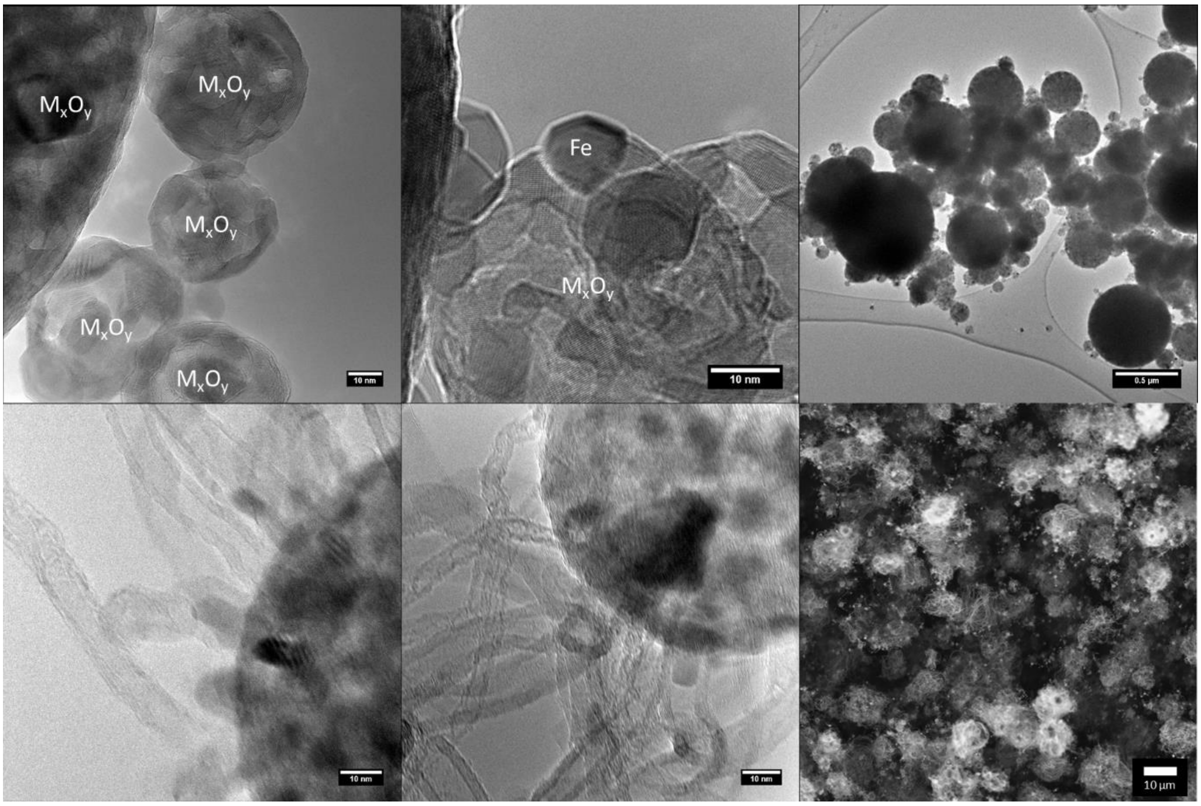

Fig. S6: HRTEM images of metal oxide core materials (top row) without CNT growth and TEM images (bottom row) with CNT growth.

Supplementary Information References

[1s] B. Graves, J. Olfert, B. Patychuk, R. Dastanpour, S. Rogak, Characterization of particulate matter morphology and volatility from a compression-ignition natural-gas direct-injection engine, Aerosol Sci. Technol. 49 (2015) 589–598. doi:10.1080/02786826.2015.1050482.

[2s] N. Tajima, N. Fukushima, K. Ehara, H. Sakurai, Mass range and optimized operation of the aerosol particle mass analyzer, Aerosol Sci. Technol. 45 (2011) 196–214. doi:10.1080/02786826.2010.530625.

[3s] W.D. Kim, J.Y. Ahn, D.G. Lee, H.W. Lee, S.W. Hong, H.S. Park, S.H. Kim, Tailoring the carbon nanostructures grown on the surface of Ni-Al bimetallic nanoparticles in the gas phase, J. Colloid Interface Sci. 362 (2011) 261–6. doi:10.1016/j.jcis.2011.06.043.